JMEPEG
https://doi.org/10.1007/s11665-022-07249-7

©ASM International
1059-9495/$19.00

TECHNICAL ARTICLE

Investigating the Microstructural, Mechanical, and Tribological Properties of NiCrBSi High-Velocity Oxygen Fuel and High-Pressure High-Velocity Oxygen Fuel Coatings

Ali Eskandari, Ali Shafyei, Fatemehsadat Sayyedan, Mohammadreza Afsous, and Mohsen Adamzadeh

Submitted: 7 January 2022 / Revised: 8 June 2022 / Accepted: 29 June 2022

In this study, the effect of the coating process and heat-treatment cycles on the microstructural, mechanical, and tribological properties of NiCrBSi coatings deposited by High-Velocity Oxygen Fuel (HVOF) and High-Pressure High-Velocity Oxygen Fuel (HP-HVOF) techniques were investigated. The metallographic assessments, Energy Dispersive x-ray Spectroscopy (EDS), x-ray Diffraction (XRD), microhardness measurements, and nano-indenter tests were run on the as-sprayed and heat-treated coatings. The tribological properties were assessed using ball-on-disk wear test. The worn surfaces were observed using Scanning Electron Microscopy (SEM) and Atomic Force Microscopy (AFM). The results of the nano-indentation test indicated that the Young's modulus of the coatings increased through the heat-treatment up to 20%. The tribological measurements indicated that the wear resistance of the as-sprayed HP-HVOF coating was 60% greater than that of the HVOF due to improved metallurgical properties and optimal hardness to Young's modulus ratio. Moreover, heat-treatment of the HVOF coatings at 950 °C for 1 h increased the wear resistance up to 50%, while increasing temperature up to 1000 °C caused a decrease in the wear resistance because of the considerable reduction in the microhardness. The worn surface studies revealed the existence of tribo-oxidation and abrasion as the main wear mechanisms involved in all samples.

Keywords heat-treatment, high-velocity oxy-fuel (HVOF), high-pressure high-velocity oxygen fuel (HP-HVOF), NiCrBSi coatings, wear resistance

1. Introduction

Nickel-based coatings are mainly applied on the surface of the engineering components exposed to wear, corrosion, and oxidation from medium to high temperatures. These alloys are widely used in chemical, aerospace, oil, and automotive industries (Ref 1, 2). NiCrBSi is a well-known self-flux nickel-based alloy with desired properties and characteristics. This alloy is formed by adding Cr, B, Si, and C to Ni, the parent metal. Laser cladding and thermal spraying are the two common procedures for applying these alloys. Industrial applications of thermally-sprayed NiCrBSi and Ni–B-Si coatings accompanied with post treatment initiated in 1955 (Ref 3-5). High-Velocity Oxygen Fuel (HVOF) is a thermal spraying technology to deposit coatings with high resistance to wear and corrosion. The High-Pressure HVOF (HP-HVOF) is another coating technology with higher particles' shot speed compared to HVOF to develop coatings with modified microstructural features.

These two processes are categorized as the thermal spraying processes with the same coating mechanism, but different spraying parameters. The combustion chamber pressure in the HP-HVOF process reaches a value of 3 MPa which is much more than that of the HVOF. This parameter can dramatically influence the particles' temperature and velocity which affects the microstructure followed by the coatings characteristics. In general, high particles' velocity results a dense deposit with low porosity and good adhesion to the substrate. In this technology, the particles are less exposed to air because of their high velocity. It is expected that the HP-HVOF technique leads to the formation of a dense coating with less oxidation, decarburization, and decomposition (Ref 6).

Post heat-treatment enhances the performance of thermally-sprayed coatings by decreasing the porosity and increasing the cohesion and the adhesion strength, and thus an improved wear resistance (Ref 7, 8). The three methods, namely furnace, flame and laser are adopted in post treatment (Ref 9-14). Among these, the flame method is of low accuracy and the reproducibility, and the results strongly depend on the operator's precision and skill. In contrast, the laser method is of high accuracy with narrow heat-affected zone, but less cost effective. Finally, the furnace is the simplest method with both acceptable precision and reproducibility compared to the two others.

There are many studies on the effect of the coating process and thermal treatment on the tribological properties of the coatings through furnace method. As it is expected that changes in spraying parameters would yield a more quality coating,

Ali Eskandari, Ali Shafyei, Fatemehsadat Sayyedan, Mohammadreza Afsous, and **Mohsen Adamzadeh**, Department of Materials Engineering, Isfahan University of Technology, Isfahan 84156-83111, Iran. Contact e-mail: alieskandari.iut.1389@gmail.com.

Published online: 25 August 2022

some efforts have been made to obtain coatings with better characteristics, in terms of both microstructural and mechanical properties. The temperature of heat-treatment in the range of 1025-180 °C with duration of 5-30 min has been assessed by many researchers (Ref 8-13). It has been found that improving the coatings' properties cannot be achieved thoroughly with short cycles of heat-treatment. On the other hand, the metallurgical properties and wear behavior of nickel-based HVOF and HP-HVOF coatings have not yet been assessed and compared in the available studies.

The researchers in this article seek to propose re-melted coatings with improved metallurgical properties and wear resistance through heat-treatment. Moreover, the effects of microstructure, hardness, and Young's modulus on the tribological properties of NiCrBSi coatings deposited by HVOF and HP-HVOF techniques have been assessed by considering the coating parameters and thermal-treatment cycles.

2. Experimental Procedure

2.1 Sample Preparation and Coating Process

Disk-shaped specimens made of AISI 316L stainless steel with 50 mm diameter and 5 mm thickness were prepared as the substrates. The chemical composition of the substrate is 18%Cr, 14%Ni, 2.5%Mo, 1.5%Mn, 0.5%Si, 0.1%n and Fe as Bal. The specimens were sand blasted by Al_2O_3 particles of 0.9-1.1 mm diameter. The Colmonoy88 NiCrBSi powder with an average particle size of 45 μm, the particle size distribution of 25-60 μm, and chemical composition is 15.2%Cr, 4%B, 4.8%Si, 4.45%Fe, 4.5%W, 0.05%C and Ni as Bal.

HVOF and HP-HVOF techniques were employed to deposit the powder on the substrates. The samples were named using the following scheme: Technique/Temperature/Time. For example, H950-1 denotes the sample made with HVOF, and heat treated at 950 °C for 1 h, H950-2 denotes the sample made with HVOF, and heat treated at 950 °C for 2 h, H1000-1 denotes a sample made with HVOF, and heat treated at 1000 °C for 2 h. Likewise, HP950-1 denotes a sample made with HP-HVOF, and heat treated at 950 °C for 1 h, and HP1000-1 denotes a sample made with HP-HVOF, and heat treated at 1000 °C for 1 h. After coating process, the first group were heat-treated at 950 °C for 1, 2 and 4 h and the others at 1000 °C for the same time intervals in a tube furnace with an inert atmosphere followed by being air cooled. The specimens were labeled based on the spraying technique and heat-treatment according to Table 1.

Table 1 Spraying process parameters

Parameters	HVOF	HP-HVOF
Gun	HV-2000	JP-5000
Oxygen flow rate, l/min	1000	1800
Fuel flow rate, l/min	22	45
Spray distance, mm	300	300
Carrier gas	Argon	Argon
Powder feed rate, g/min	60	80
Combustion pressure, bar	7	28

2.2 Coating Characterization

The cross-sectional microstructure and elemental analysis of the coatings were characterized using the scanning electron microscopy (SEM Philips, model M130) equipped with the energy dispersive spectroscopy (EDS). The specimens were grounded by SiC sand-paper numbered from 120 to 1200 and polished by alumina slurry and then etched in the solution of $1HCl:10HNO_3:10H_2O$ (vol.%) to appear the microstructure. The phase composition analysis of the original powder, as-sprayed HVOF and HP-HVOF samples, and heat-treated coatings were assessed using the x-ray diffraction (XRD) analysis (Philips, model Xpert-MPD). The XRD analysis was run by applying the copper x-ray tube (λ-K, $\alpha_1 = 0.1540598$ nm) within 2θ range of 30°-100°.

The microhardness measurement was made on the cross section of the coatings by applying the Buehler microhardness tester ($HV_{0.1}$ with a 15 s dwell time). The reported hardness numbers were the average values of ten indentations in different points of the samples. Coating stiffness along the cross section was evaluated using the nano-indentation test with a maximum load of 0.1 N, by applying the compact platform of NHT B-j87 Berkovich indenter. The reported results were the average values of five tests performed.

The tribological behavior of both as-sprayed and heat-treated coatings were assessed by running the ball-on-disk test (Wear co., model WP50) according to ASTM G99 standard test method. Each test was repeated for three times on all of the specimens and the average value was reported. The coated disks were subjected under load of 50 N, the sliding distance of 1000 m, and the linear velocity of 0.1 m/s to evaluate wear resistance. The Al_2O_3 ball with a hardness of 1800 Hv was selected as the counterpart due to its high wear resistance. It is worth to mention that in some pumps; the NiCrBSi-coated plunger is subjected to wear against the cylinder. Next to determining the wear rate, the wear track of the worn surfaces was studied by SEM/EDS and atomic force microscope (AFM), by applying the Bruker model NHTXS/N: 01-03,119. A thickness of 100 μm from the original coating thickness of 350 μm was shaved in tribological assessments.

3. Results and Discussion

3.1 Microstructural Observations

Figure 1(a) and (d) represents the splat boundaries, porosity, and some un-melted particles in the cross-sectional microstructure of the as-sprayed coatings. These defects are more apparent in the coatings sprayed by HVOF than those in the HP-HVOF due to the lower particles' velocity. The porosities (dark contrast spots) at the coating/substrate interface of the as-sprayed specimens result lower adhesion strength. Some differences in the size and distribution of the porosities in the as-sprayed H and HP coatings were observed. The porosity size in the HVOF as-sprayed coating was far bigger than that of the HP-HVOF. It is evident that the HP-HVOF process leads to coatings with a more uniform porosity distribution. The pores with long horizontal orientation were formed due to the impact of both molten and semi-molten particles next to their deformation and contraction (Fig. 1a and b). These pores represent the brittle lamellar microstructure nature that corresponds to the coating's performance (Ref 9).

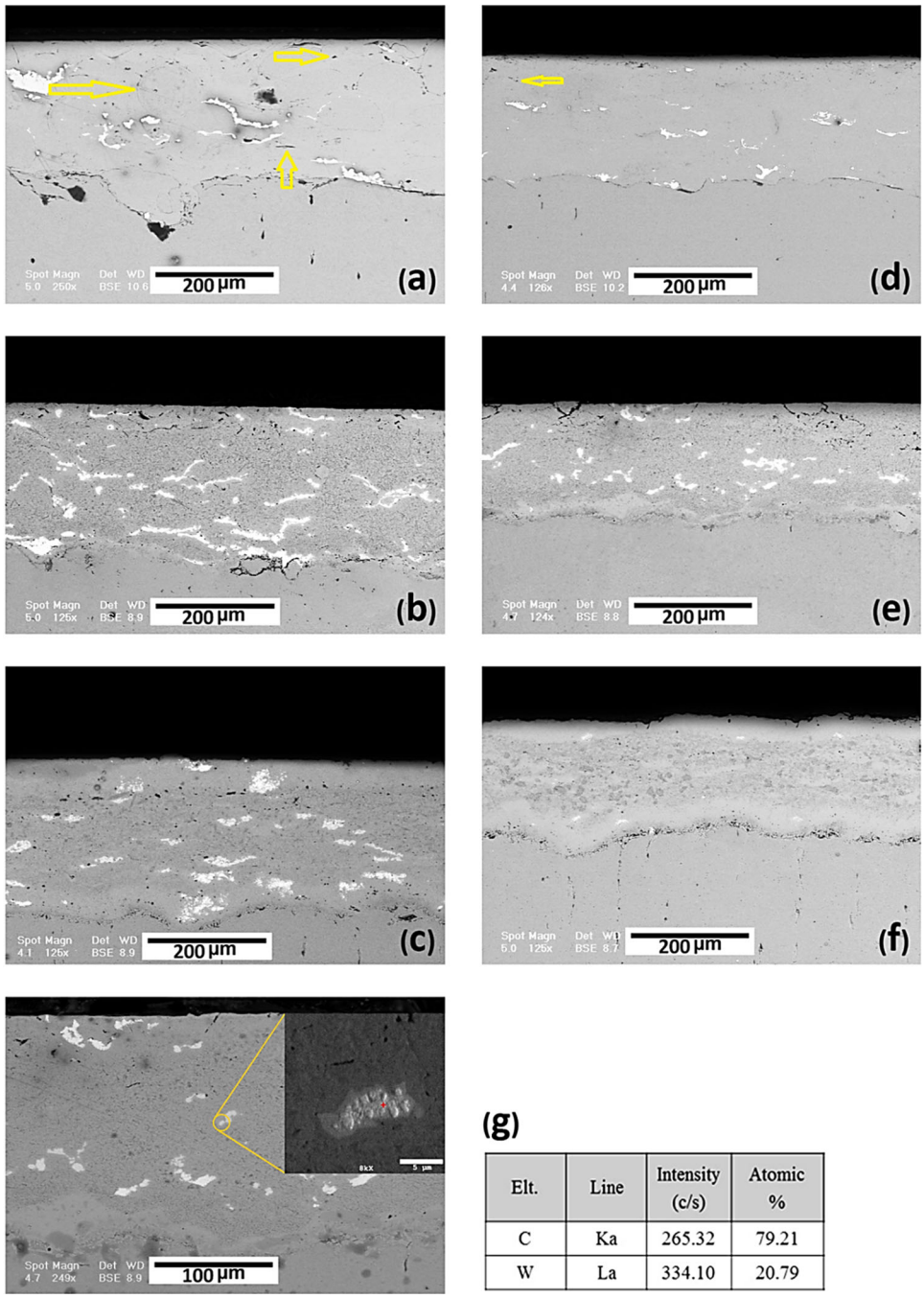

(g)

Elt.	Line	Intensity (c/s)	Atomic %
C	Ka	265.32	79.21
W	La	334.10	20.79

Fig. 1 Cross-sectional microstructure of H (a), H950-1 (b), H1000-1 (c), HP (d), HP950-1 (e), and HP1000-1 (f), EDS analysis of WC in the coating's microstructure (g)

The splat boundaries and porosities raised from the formation of the melt phase and diffusion process during heat-treatment have been decreased significantly in the heat-treated coatings compared to the as-sprayed specimens. It has been reported that the formed molten phase during heat-treatment is the Ni-Ni_3B (known as a low-temperature eutectic). The wettability and the surface tension of such a low-temperature eutectic can be efficiently controlled by the boron, as forming the hard phases, and silicon, acting as a deoxidizing and fluxing agent (Ref 15, 16).

In the first stage of the heat-treatment, a reduction in porosity could occur through the capillary motion of the low viscosity melt (eutectic) in the mixed zone along the solidus and liquidus. This melt motion could sufficiently wet and fill the voids' surface (Ref 9). Porosity percentage was calculated in the CLEMEX image analysis s/w environment. The porosity percentage of the as-sprayed H and HP coatings were approximately 3.0 and 1.0%, respectively. Shrestha et al. estimated the porosity percentage of the fused NiCrBSi coatings to be 0.2-0.3% (Ref 17), while other researchers revealed that the same was around 2% (Ref 11). Their results indicated that the complete densification could not occur even after heat-treatment. The porosity percentage may decrease considerably due to the formation of porosities near the regions

with the high volumes of carbides and the porosities being surrounded by the precipitates.

As observed in Fig. 1(b), (c), (e), and 1f, three distinct regions could be pin-pointed in the cross section of the heat-treated coatings, namely: (1) the upper layer, (2) the intermediate layer, and (3) the layer named the dilution zone, near the coating/substrate interface, which can enhance the adhesion strength of the coating to the substrate.

The diffusion of the elements due to the existence of concentration gradient between the coating and the substrate forms the dilution zone. This phenomenon, that occurs between the substrate and the heat-treated coatings, has been described by Gonzalez et al. (Ref 18).

The white areas in the microstructure indicated tungsten carbide particles, the existence of which would be proved by the EDS and XRD analyses, Figs. 1g and 2, respectively.

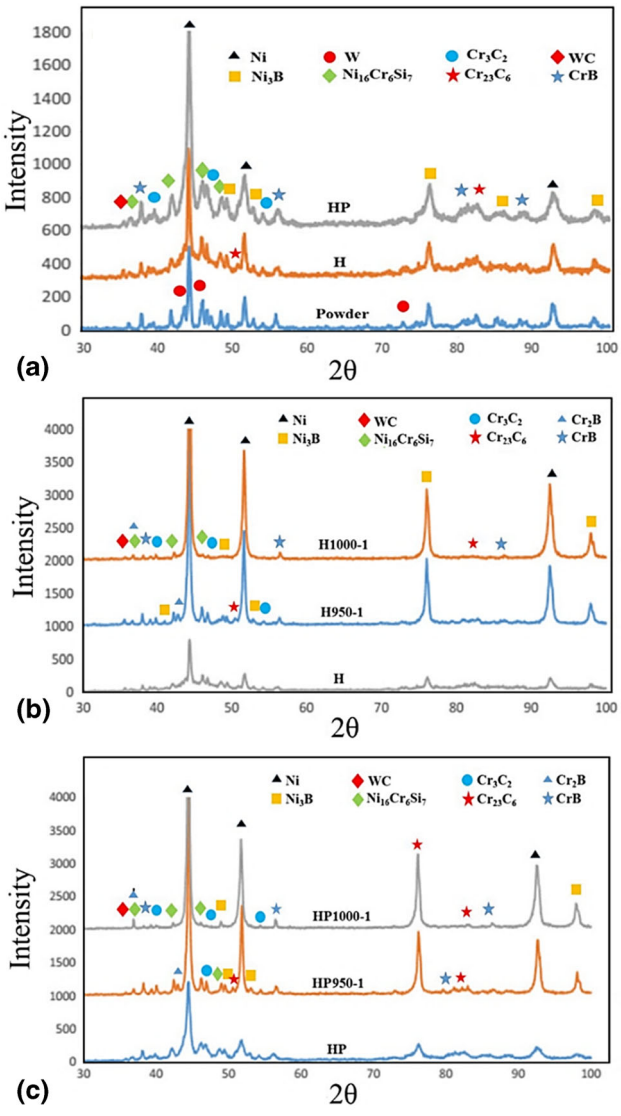

Fig. 2 XRD patterns of the powder and as-sprayed specimens (a), as-sprayed and re-melted specimens developed by HVOF (b), and as-sprayed and re-melted specimens obtained from HP-HVOF (c)

3.2 XRD Analysis

The structural features and phase composition of the powder and as-sprayed specimens were compared with those of the heat-treated specimens through XRD patterns (Fig. 2). The phase composition of the powder Fig. 2(a) consisted of the Ni solid solution, the eutectic phase Ni_3B, carbides like $Cr_{23}C_6$ and Cr_3C_2 and CrB, and $Ni_{16}Cr_6Si_7$. These borides and carbides are the strengthening phases in the matrix. These phases enable the coatings to resist against the counterpart and tend to narrow the wear grooves (Ref 19). According to the XRD patterns of the as-sprayed specimens shown in Fig. 2(a), it is assumed that a certain volume of WC is originated from the spraying process due to the high temperature of the coating process and also, the presence of tungsten and carbon in the powder composition. In this study, it was found that the changes in the coating process had no effects on the phase composition.

XRD patterns of the as-sprayed specimens revealed a curvature appeared at $2\theta = 40°\text{-}50°$ and broader XRD lines, indicating the formation of the amorphous phases during the coating processes. The results reported by Chen et al. indicated that the cooling rate of the particles in thermal spraying was within the range of 10^{-6}-10^{-8} s^{-1}, which could lead to the formation of the amorphous phase, influencing the Young's modulus and hardness, and thus, affecting the wear resistance (Ref 20). Based on the theory of kinematic, the XRD peaks could be broadened due to the presence of the lattice defects in great count or reduction in the crystallites' size to less than 1 μm (Ref 21).

The attenuation and broadening of the diffraction peaks could be associated with adding boron and the increase in the glass-forming ability (GFA) of the Ni-based alloys. Adding boron decreases the melting temperature and increases the GFA, leading to an enhanced stability of the super-cooled liquid against the crystallization process. The diffraction broadening is also probable, because both HVOF and HP-HVOF spraying processes could be considered as a rapid heating and cooling process (Ref 22).

The critical transition temperature for NiCrBSi coatings falls within the range of 300-500 °C (Ref 23). Heat-treatment at 950 and 1000 °C for one hour transformed some of the CrB to Cr_2B in all as-sprayed coatings. Boron and nickel could form Ni_3B due to the formation of the molten phase and increase the diffusion rate during the heat-treatment.

A contraction of curvature in the heat-treated specimens can be related to the crystallization during the heat-treatment (Fig. 2b and c) (Ref 23). Different levels of crystallinity due to the heat-treatment could be one of the possible reasons for the slight curvature shift in the as-sprayed and re-melted coatings (Ref 12, 24). The peak intensity of the γ-Ni solid solution and Ni_3B compositions due to the equilibrium reaction in the heat-treated specimens was tenfolds greater than that of the as-sprayed ones.

3.3 Microhardness Test

The measured microhardness along the thickness of the coatings is shown in Fig. 3, where all coatings are of similar behavior. Compressive stress, cohesion and microstructure would affect the microhardness, and consequently the tribological properties (Ref 25). Precipitates of Ni_3B and Cr_2B can influence the microhardness. The results indicated that the

specimen microhardness of the HP coating was 1.1 times greater than that of the H specimen due to the superior compressive stress and cohesion obtained from the HP process. Heat-treated coatings had lower hardness compared to the as-sprayed ones, which is explained by the finer microstructure and higher compressive stress of the as-sprayed coatings compared to the heat-treated ones. Researchers have revealed that the heat-treatment coarsens the microstructure and relieves the compressive stress. Where the applied load for the hardness measurement (100 g) is light, indicating the absence of coating porosity effect on the as-sprayed zone (Ref 25, 26).

Stress relieving phenomenon during heat-treatment could be another reason for the decrease in hardness in the re-melted specimens. Heat-treatment at high temperatures commonly corresponds to the significant decrease in the microhardness. As observed in Fig. 3, the alteration trends of as-sprayed coatings are stepwise at the coating/substrate interface, while this trend occurred by a gentle and gradual decrease in the case of the re-melted coatings. These gradual changes are due to the formation of the dilution zone at the coating/substrate interface during the heat-treatment.

The high re-melting temperatures correspond to the smooth rate of change in the microhardness as a result of more diffusion at the coating/substrate interface (see Fig. 3). The dilution layer hardness, depending on its chemical composition, is somewhat between the coating and the substrate hardness, indicating that the closer the chemical composition of the substrate, the closer the hardness of the substrate. It is obvious that the heat-treatment can reduce the substrate microhardness.

3.4 Nano-Indentation Test

Hardness and Young's modulus' values of the coatings were determined by adopting the Nano-indentation method. The Young's modulus was determined by measuring the force and displacement of the indenter, simultaneously. Young's modulus depends on the chemical composition, microstructure, cohesion, and anisotropy (Ref 27). Young's modulus of the heat-treated coatings were estimated at least 1.2 times greater than that of the as-sprayed coatings due to the cohesion enhancement through the re-melting process (Ref 24).

The grain boundary strength may increase the Young's modulus. The presence of the amorphous phase in the as-sprayed coating could decrease the Young's modulus. The coatings' wear behavior cannot be interpreted solely by their hardness or Young's modulus. The wear resistance of the coating could be predicted efficiently by the ratio of hardness to Young's modulus (H/E), which usually has an optimal value, where the wear resistance is the highest (Ref 28).

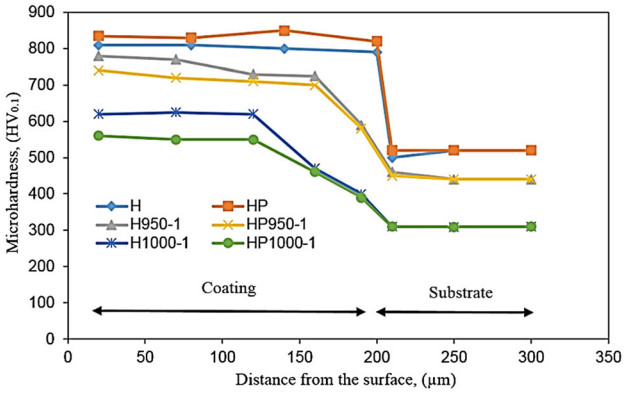

Fig. 3 Microhardness variation of H, H950-1, H1000-1, HP, HP950-1, and HP1000-1 specimens corresponding to the coating thickness

According to Table 2, the heat-treatment at 950 °C for 1 h leads to an increase in HVOF coatings' Young's modulus up to 20%, while this heat-treatment cycle tends to increase the HP-HVOF coatings' Young's modulus only up to 3%. This increase is due to the presence of more structural defects after heat-treatment in the HVOF coating compared to the HP-HVOF one. Thus, the heat-treatment of the HVOF coating could reduce the defects volume, leading to more enhancement in the Young's modulus.

The results revealed that the heat-treatment at 950 °C for 1 h decreased the HVOF and HP-HVOF coatings' hardness up to 21 and 42%, respectively. This decrease could be due to the reduced compressive stresses. It is assumed that the coatings sprayed through the HP-HVOF process is of high compressive residual stress as a result of the high velocity of the particles and also, the high cooling rate. In their thermodynamic sense, these coatings are of high driving force to relieve the residual compressive stress during the re-melting process. The thermal energy released from the heat-treatment leads to the enhancement of cohesion and splat boundaries' elimination (Ref 29), next to degrading the compressive stresses. As observed in Fig. 1, the HP-HVOF coating is of high cohesion in comparison with the HVOF coating, consequently, the thermal energy resulting from the heat-treatment could be more contributive in decreasing the compressive stresses. These facts could explain the reason why the HP-HVOF coatings are of lower hardness after the re-melting process.

3.5 Tribological Assessment

The weight loss diagrams of both as-sprayed HVOF and HP-HVOF coatings are shown in Fig. 4(a), where the HVOF heat-treated coatings at 950 °C undergo less weight loss, consequently, more wear resistance in comparison with the as-sprayed coatings. The H950-1 specimen exhibited the best wear resistance among the coatings through the HVOF technique, while heat-treatment at 1000 °C, reduced this wear resistance due to the high decrease in hardness after heat-treatment because of stress relief (Fig. 3).

Unlike the coatings sprayed by the HVOF technique, that the heat-treatment at either 950 °C or 1000 °C decreased the wear resistance of the coatings deposited through the HP-HVOF technique, is evident in Fig. 4b. As observed in Figs. 4(a) and (b), the wear resistance was decreased with an increase in the heat-treatment temperature, where time was fixed and vice versa.

The weight loss results of all specimens in both techniques is shown in Fig. 5(a), where the coating technique affects the

Table 2 Mechanical properties of as-sprayed and re-melted coatings

H/E	E, GPa	H, GPa	H, Hv	Specimen
0.067	170.20 ± 8.5	11.5 ± 1.1	1000 ± 56	H
0.055	218.14 ± 9.2	12.2 ± 0.7	1100 ± 49	HP
0.044	205.27 ± 3.5	9 ± 1.0	800 ± 34	H-950–1
0.031	225.67 ± 6.8	7 ± 0.2	720 ± 12	HP-950–1

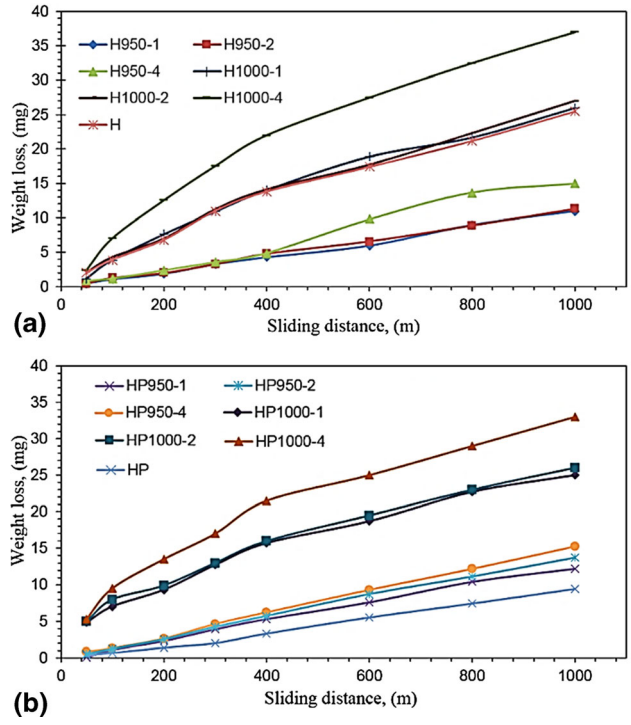

Fig. 4 Weight loss diagrams of as-sprayed HVOF (a) and HP-HVOF (b) coatings after the ball-on-disk wear test at 50 N load and the sliding velocity of 0.1 m/s, in comparison with the Al_2O_3 ball counterpart

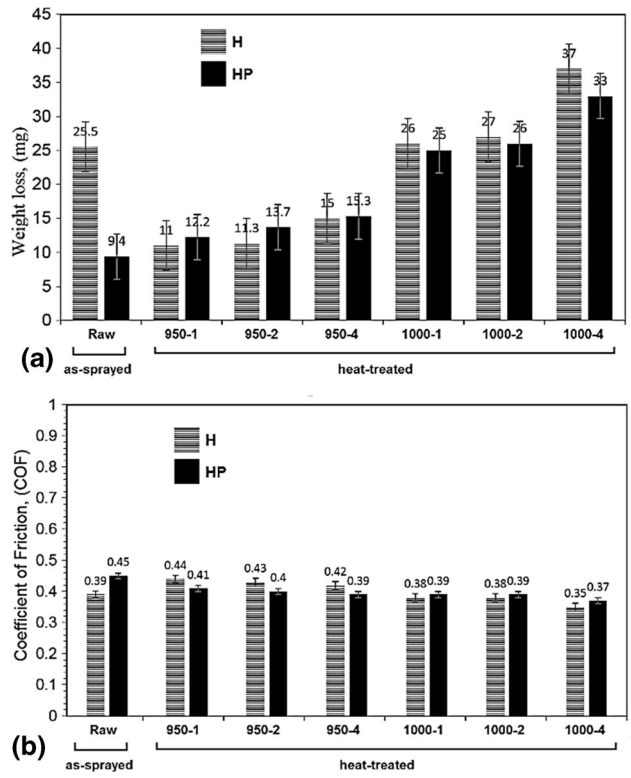

Fig. 5 Weight loss (a) and COF (b) comparison of all specimens after the ball-on-disk wear test at 50 N load and the sliding velocity of 0.1 m/s

wear characteristics, and the heat-treatment conditions can enhance/weaken the tribological behavior. According to this figure, the as-sprayed HP coating revealed the best wear resistance among all specimens, and the weight loss of the H specimen was five times more than that of the HP one. The heat-treatment of HVOF coatings at 950 °C for 1 h would increase the wear resistance up to 50%, indicating superior wear resistance in comparison with similar heat-treated HP coatings of HP950-1. According to the comparison in Table 2 and the diagrams presented in Fig. 5(a), the deviation from the optimal value of H/E ratio reduces the wear resistance. This makes the as-sprayed H specimen to have the maximum H/E ratio with the lowest wear resistance. Due to the lack of sufficient cohesion, the splat delamination and deep grooves cannot be avoided at high hardness of the coating, thus, more weight loss. Presence of the high volumes of porosities and non-uniform distribution therein in the H specimen corresponds to its poor performance and low wear resistance. The HP, HP950-1 and H950-1 coatings were of a similar H/E ratio, which corresponds to their similar weight loss volume.

The coefficient of friction (COF) values of all coatings in both approaches of as-sprayed and heat-treated are shown in Fig. 5b. Compared with the weight loss volumes (Fig. 5a), it was found that the COF increases with an increase in the wear resistance that corresponds to the decrease in the weight loss. This increase in COF could be related to the stable oxide layer formation that protects the surface from potential damage.

The ascending trend of the weight loss diagram in Fig. 4 (associated with the increase in the wear rate) corresponds to the decrease in the COF values. The high gradient in the weight loss diagram indicated that either the oxide layer was unstable or the oxide layer formation rate was less than that of the destruction rate (Ref 30, 31). These oxides act as the transfer layer that hinders the direct contact between the counterpart and the coating during the wear test (Ref 19).

It is notable that the presence of the oxide layers cannot necessarily generate the low frictional forces leading to less surface damage. The oxide layers determine the COF at the wear front (Ref 18). Another parameter influencing the COF value is the coatings' hardness, which can also affect the tribological performance (Ref 20).

The wear track micrographs related to the as-sprayed HVOF, heat-treated H950-1 and H1000-1 NiCrBSi coatings at two magnifications are shown in Fig. 6. Scratches with splats delamination are presented by the arrows in Fig. 6a. The AFM analysis of the as-sprayed H coatings' wear track (Fig. 7a) revealed the parallel scratches, by introducing the micro-cracking as the abrasive wear mechanism.

The pores and splat boundaries in the as-sprayed H coating represent a low cohesion strength, allowing the crack growth to pull out the whole splat from the coating's surface (Ref 22). This could reduce the wear resistance. The fatigue damage mechanism controls the wear behavior in thermally-sprayed coatings, especially when the poor cohesion energy is produced (Ref 32, 33). This process, named *splat delamination*, is unique to fatigue damage mechanism.

The wear track shown in Fig. 6b is of dominantly smooth surface with less scratches. The AFM analysis image of the H950-1 coating (Fig. 7b) exhibits parallel narrow and shallow grooves. The weight loss (Fig. 5a) and wear track (Fig. 6) comparisons indicate the existence of matrix micro-cutting which is assumed as the main abrasive wear mechanism, where the low count of the scratches and the parallel smooth grooves

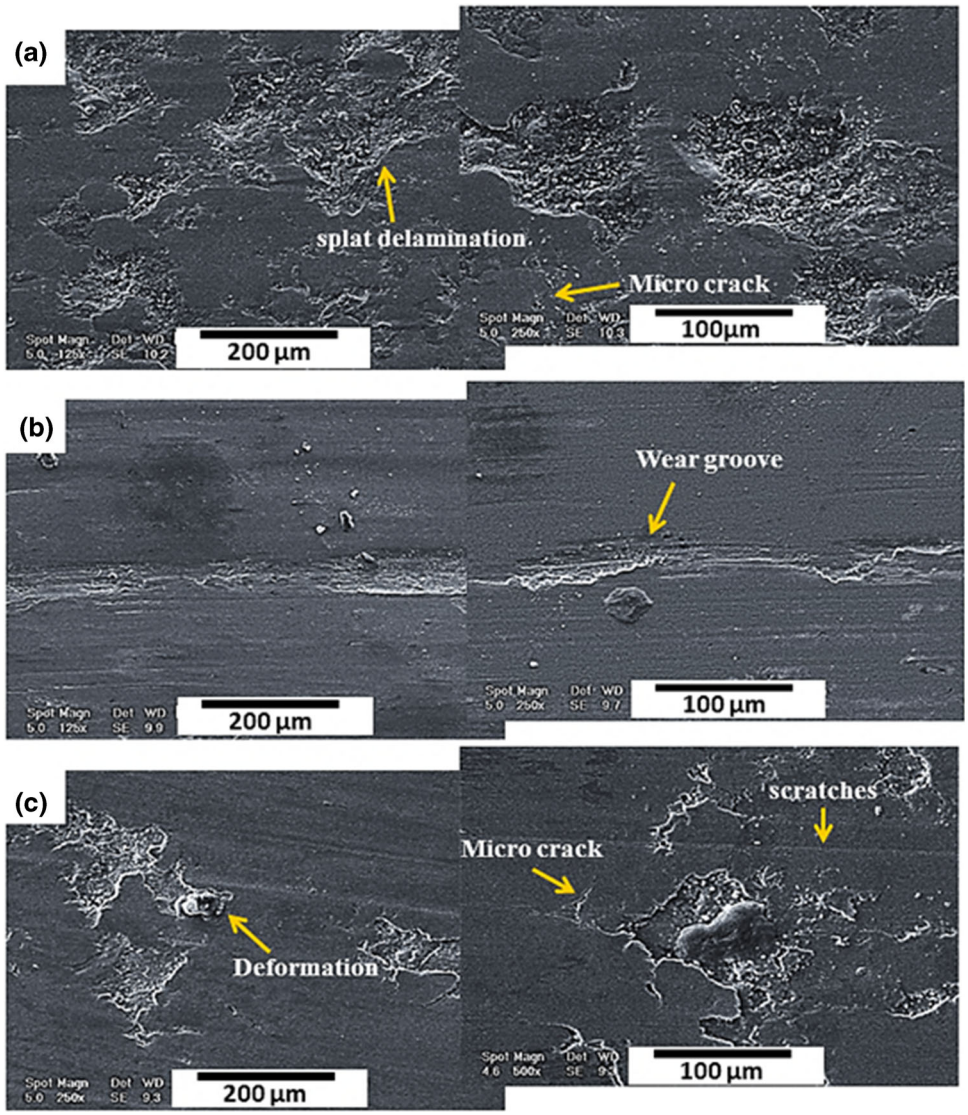

Fig. 6 SEM micrographs of the wear tracks on the HVOF coatings: as-sprayed H (a), H950-1 (b), and H1000-1 (c)

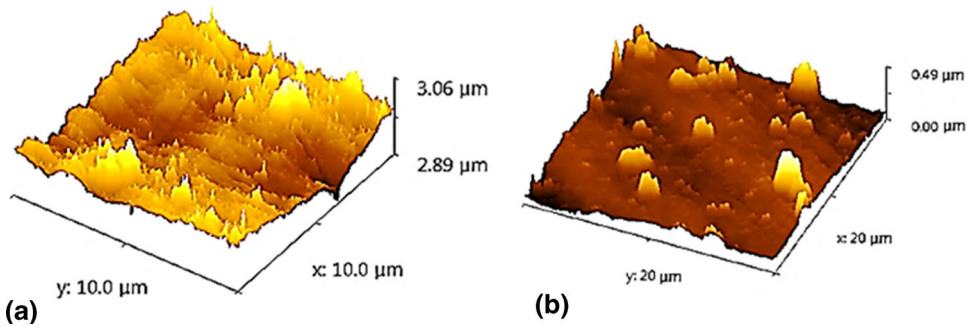

Fig. 7 AFM analyses of the wear track of the HVOF coatings: (a) as-sprayed specimen H, (b) H950-1 specimen

indicate high wear resistance of this specimen. Comparing the figures of the as-sprayed H coating with those of the heat-treated coating reveals that the depth and the wear grooves' count decrease in the heat-treated specimen. The heat-treated coating had a smoother surface, confirmed by the low weight loss in this specimen (Fig. 4).

Deformation, micro cracks, and wear grooves evident in the wear track marked by the arrows in Fig. 6 revealed the existence of both adhesive and abrasive wear mechanisms. Also, the formation and propagation of micro cracks among the splats could be indicative of the delamination wear (Ref 23). The cyclic loading during the wear test does increase the dislocations density beneath the exposed surface, leading to the

local increase in the hardness. The high increase in the local hardness in the near surface regions and the accumulation of dislocations could lead to the formation of some pores just beneath the worn surface, the concentration of which, form subsurface cracks, leading to possible lamellar wear (Ref 34).

The results of the EDS elemental analysis run on the debris accumulated form the wear of the as-sprayed H, heat-treated H950-1 and H1000-1 specimens accompanied with the XRD pattern of the debris gathered through the wear of the as-sprayed H coating are shown in Fig. 8. These data correspond to the wear tracks are shown in Fig. 6. A close look on the contents of Fig. 8 reveals the existence of a considerable volume of nickel oxide (NiO) and iron oxide (Fe_2O_3) in the debris. The findings here correspond to those obtained by some researchers (Ref 5, 11, 12, 35-37). As to HVOF coatings, the scratches on the wear tracks form an abrasive wear mechanism.

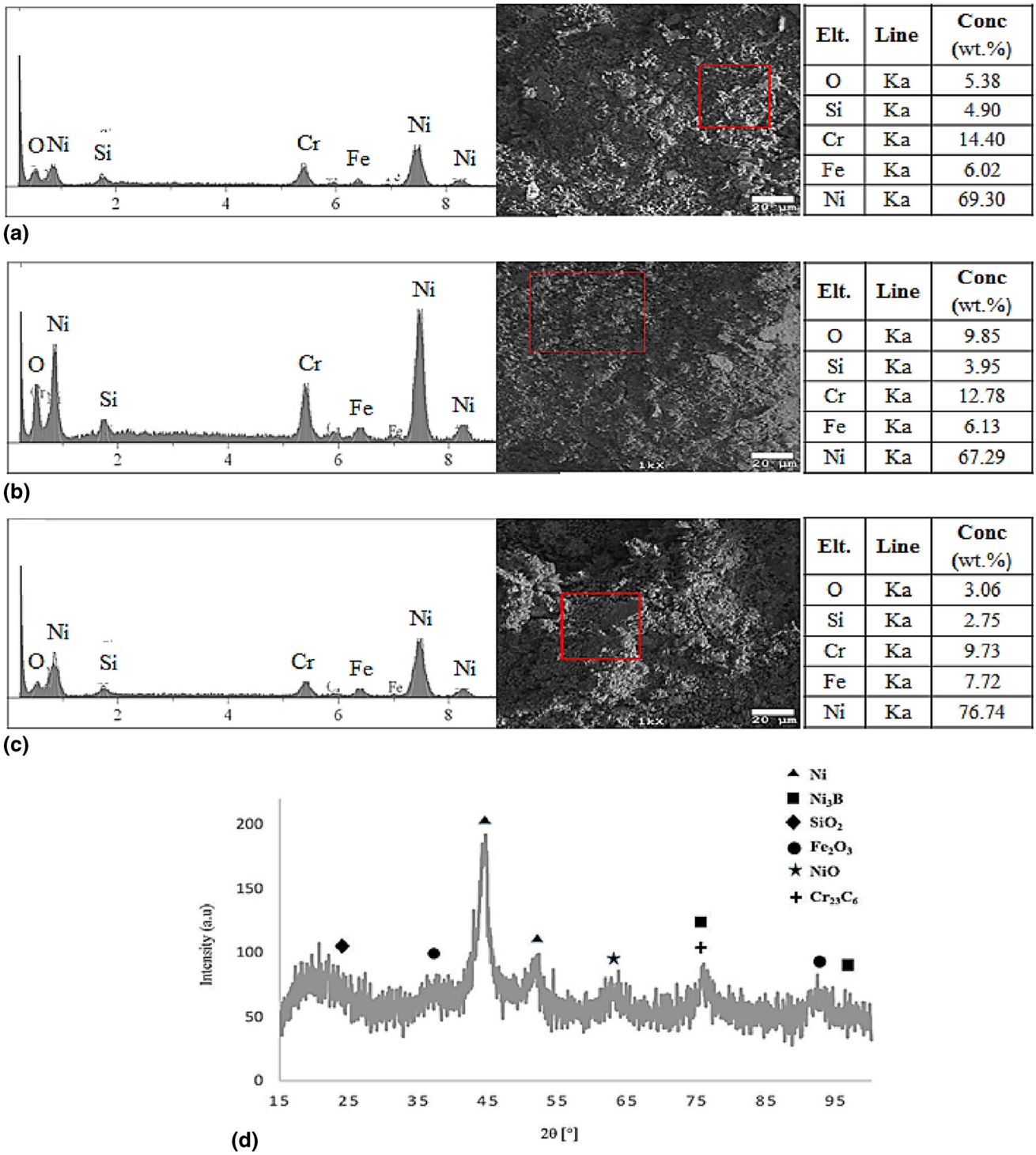

Elt.	Line	Conc (wt.%)
O	Ka	5.38
Si	Ka	4.90
Cr	Ka	14.40
Fe	Ka	6.02
Ni	Ka	69.30

Elt.	Line	Conc (wt.%)
O	Ka	9.85
Si	Ka	3.95
Cr	Ka	12.78
Fe	Ka	6.13
Ni	Ka	67.29

Elt.	Line	Conc (wt.%)
O	Ka	3.06
Si	Ka	2.75
Cr	Ka	9.73
Fe	Ka	7.72
Ni	Ka	76.74

Fig. 8 EDS analyses of the debris of the as-sprayed H (a), heat-treated H950-1 (b), and H1000-1 (c) coatings. XRD pattern of the debris gathered through the wear of the as-sprayed H coating (d)

According to the EDS results (Fig. 8a-c) and the XRD pattern (Fig. 8d) of the debris, the tribo-oxidation mechanism has been occurred during the sliding contact, indicating the three-body wear mechanism occurred. In fact, oxide particles stuck between two surfaces cause abrasion.

The wear track morphologies of the as-sprayed HP, heat-treated HP950-1 and HP1000-1 NiCrBSi coatings are shown in Fig. 9. The wear track of the as-sprayed coating exhibited scratches, smooth wear grooves and some pulled out particles, presented by the arrows in (Fig. 9a). In the AFM analysis, the images of scratches are observed in small quantities. On the worn surface of the HP specimen, the parallel narrow and shallow wear grooves are observed, which could be attributed to the abrasive mechanism as the main controlling mechanism. In comparison with the heat-treated HP coating, the wear tracks were very smooth (Fig. 10).

Either of the heat-treated HP950-1 or HP1000-1 coatings exhibited more severe grooves on their wear tracks (as shown by the arrows in Figs. 9(b) and (c)) in comparison with the as-sprayed specimen. In HP950-1 sample, the abrasive wear due to the parallel grooves could be regarded as the dominant wear mechanism.

The worn surfaces revealed that the grooves' size and volume in the HP1000-1 coating were more than those of the HP950-1 coating. In HP1000-1 sample, the particles pulled out from the worn surface could be attributed to the presence of porosity beneath the surface. The considerable weight loss of the heat-treated HP1000-1 coating indicated delamination as the main abrasive wear mechanism.

The EDS elemental analysis results of the HP-HVOF coatings' wear debris are shown in Fig. 11, where the presence of oxygen is evident. Surface oxidation could be due to the presence of oxygen and the high temperature at the wear front (Ref 28). These lead to the hypothesis that the tribo-oxidation phenomenon is present in the specimens.

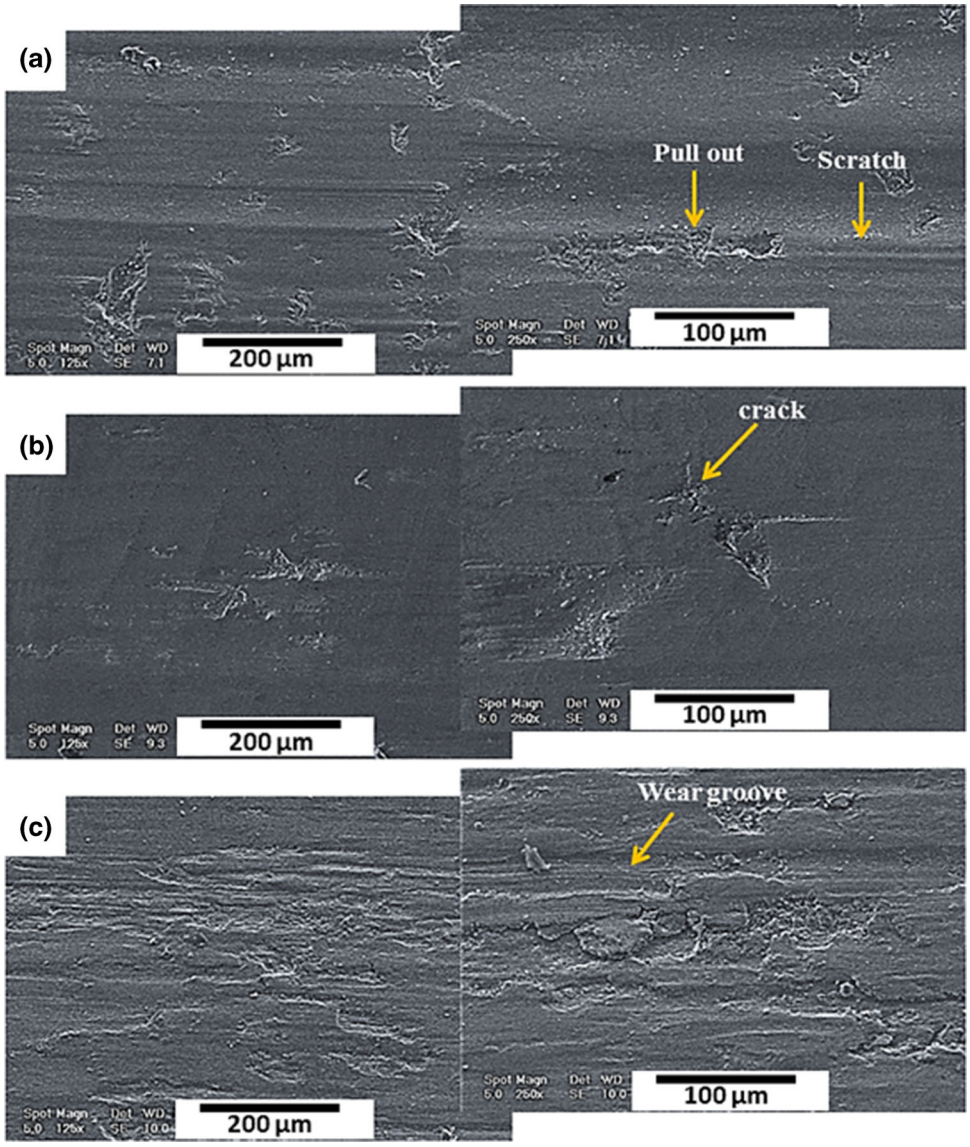

Fig. 9 SEM micrographs of the wear tracks on the HP-HVOF coatings: as-sprayed HP (a), HP950-1 (b), and HP1000-1 (c)

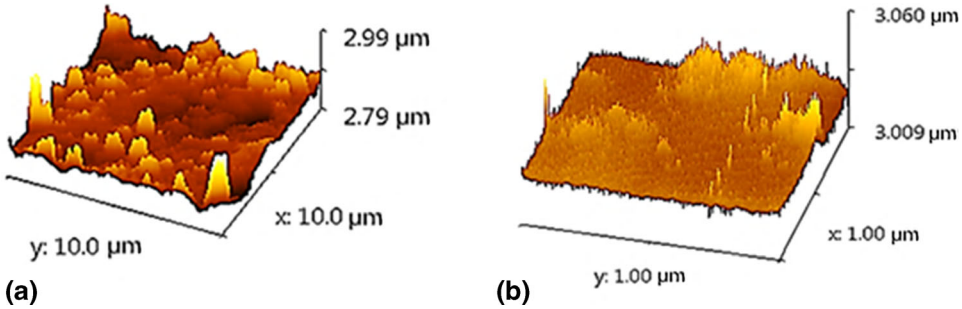

Fig. 10 AFM analyses of the wear track of the HP-HVOF coatings (a) as-sprayed specimen HP (b) HP950-1 specimen

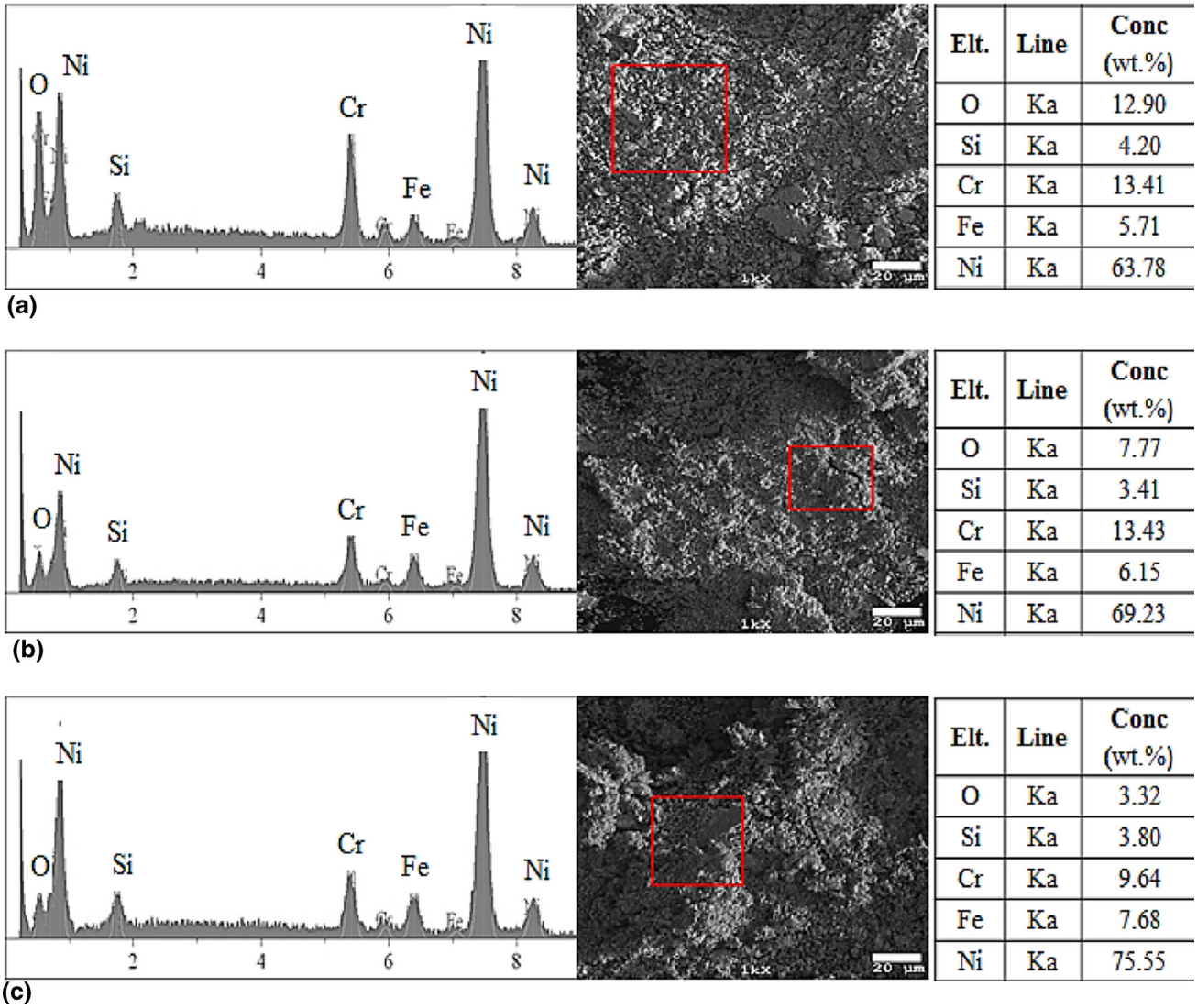

Elt.	Line	Conc (wt.%)
O	Ka	12.90
Si	Ka	4.20
Cr	Ka	13.41
Fe	Ka	5.71
Ni	Ka	63.78

Elt.	Line	Conc (wt.%)
O	Ka	7.77
Si	Ka	3.41
Cr	Ka	13.43
Fe	Ka	6.15
Ni	Ka	69.23

Elt.	Line	Conc (wt.%)
O	Ka	3.32
Si	Ka	3.80
Cr	Ka	9.64
Fe	Ka	7.68
Ni	Ka	75.55

Fig. 11 EDS analyses of the debris related to the as-sprayed HP (a), heat-treated HP950-1 (b), and HP1000-1 (c) coatings

4. Conclusions

In this research, the effect of the coating process and heat-treatment on the microstructural, mechanical and tribological properties of NiCrBSi HVOF and HP-HVOF coatings were evaluated. The main results were as follows:

1. As the result of heat-treatment, the porosity volume and splat boundaries were reduced and the dilution zone was formed due to the diffusion and formation of the molten phases. The cohesion and adhesion strengths were enhanced which subsequently increased the coatings' Young's modulus. The results obtained from the nano-indentation test revealed that the heat-treatment increased the coatings' Young's modulus up to 20%.

2. The XRD analysis revealed that there was no significant difference between the phase composition of the coatings deposited by two different techniques, namely HVOF and HP-HVOF. An amorphous phase was formed during spraying mainly due to the high cooling rate after collision.
3. 3. The as-sprayed HP-HVOF coating revealed better wear resistance compared to the as-sprayed HVOF due to its optimal H/E ratio.
4. The heat-treatment of the HVOF coatings at 950°C for 1 h increased the wear resistance up to 50%, while increasing temperature up to 1000°C caused a decrease in the wear resistance because of the considerable reduction in the microhardness.
5. 5. The SEM and EDS analyses of the wear scars and debris revealed that the abrasion and tribo-oxidation were the main wear mechanisms involved in coatings.

References

1. L.J. da Silva, C.J. Scheuer, and A.S.C. D'Oliveira, Effect of Microstructure on Wear Performance of NiCrSiBC Coatings, *Wear*, 2019, **428**, p 387–394.
2. J. Rodrıguez, A. Martın, R. Fernández, and J. Fernández, An Experimental Study of the Wear Performance of NiCrBSi Thermal Spray Coatings, *Wear*, 2003, **255**(7–12), p 950–955.
3. D. Chaliampalias, G. Vourlias, E. Pavlidou, S. Skolianos, K. Chrissafis, and G. Stergioudis, Comparative Examination of the Microstructure and High Temperature Oxidation Performance of NiCrBSi Flame Sprayed and Pack Cementation Coatings, *Appl. Surf. Sci.*, 2009, **255**(6), p 3605–3612.
4. R. Gonzalez, M. Garcia, I. Penuelas, M. Cadenas, M. Del Rocío Fernández, A.H. Battez, and D. Felgueroso, Microstructural Study of NiCrBSi Coatings Obtained by Different Processes, *Wear*, 2007, **263**(1–6), p 619–624.
5. L. Lim, Q. Ming, and Z. Chen, Microstructures of Laser-Clad Nickel-Based Hardfacing Alloys, *Surf. Coat. Technol.*, 1998, **106**(2–3), p 183–192.
6. C.R.C. Lima, R. Libardi, F. Camargo, H.C. Fals, and V.A. Ferraresi, Assessment of Abrasive Wear of Nanostructured WC-Co and Fe-Based Coatings Applied by HP-HVOF Flame, and Wire Arc Spray, *J. Therm. Spray Technol.*, 2014, **23**(7), p 1097–1104.
7. M. Oksa, E. Turunen, T. Suhonen, T. Varis, and S.-P. Hannula, Optimization and Characterization of High Velocity Oxy-Fuel Sprayed Coatings: Techniques, Materials, and Applications, *Coatings*, 2011, **1**(1), p 17–52.
8. B. Sun, H. Fukanuma, and N. Ohno, Study on Stainless Steel 316L Coatings Sprayed by a Novel High Pressure HVOF, *Surf. Coat. Technol.*, 2014, **239**, p 58–64.
9. Z. Bergant, U. Trdan, and J. Grum, Effect of High-Temperature Furnace Treatment on the Microstructure and Corrosion Behavior of NiCrBSi Flame-Sprayed Coatings, *Corros. Sci.*, 2014, **88**, p 372–386.
10. A. García, M. Cadenas, M. Fernandez, and A. Noriega, Tribological Effects of the Geometrical Properties of Plasma Spray Coatings Partially Melted by Laser, *Wear*, 2013, **305**(1–2), p 1–7.
11. H.-J. Kim, S.-Y. Hwang, C.-H. Lee, and P. Juvanon, Assessment of Wear Performance of Flame Sprayed and Fused Ni-Based Coatings, *Surf. Coat. Technol.*, 2003, **172**(2–3), p 262–269.
12. Q. Li, D. Zhang, T. Lei, C. Chen, and W. Chen, Comparison of Laser-Clad and Furnace-Melted Ni-Based Alloy Microstructures, *Surf. Coat. Technol.*, 2001, **137**(2–3), p 122–135.
13. M. Planche, H. Liao, B. Normand, and C. Coddet, Relationships between NiCrBSi Particle Characteristics and Corresponding Coating Properties Using Different Thermal Spraying Processes, *Surf. Coat. Technol.*, 2005, **200**(7), p 2465–2473.
14. X. Wang, M. Zhang, Z. Zou, and S. Qu, Microstructure and Properties of Laser Clad TiC+ NiCrBSi+ Rare Earth Composite Coatings, *Surf. Coat. Technol.*, 2002, **161**(2–3), p 195–199.
15. G.F. Vander Voort, S.R. Lampman, B.R. Sanders, G.J. Anton, C. Polakowski, J. Kinson, K. Muldoon, S.D. Henry, and W.W. Scott Jr., ASM Handbook, *Metallogr. Microstruct.*, 2004, **9**, p 44073–40002.
16. N. Kazamer, R. Muntean, P.C. Vălean, D.T. Pascal, G. Mărginean, and V-A. Serban, Comparison of Ni-Based Self-Fluxing Remelted Coatings for Wear and Corrosion Applications, *Materials*, 2021, **14**(12), p 3293.
17. S. Shrestha, T. Hodgkiess, and A. Neville, The Effect Of Post-Treatment of a High-Velocity Oxy-Fuel Ni-Cr-Mo-Si-B Coating Part I: Microstructure/Corrosion Behavior Relationships, *J. Therm. Spray Technol.*, 2001, **10**(3), p 470–479.
18. R. Gonzalez, M. Cadenas, R. Fernandez, J. Cortizo, and E. Rodríguez, Wear Behaviour of Flame Sprayed NiCrBSi Coating Remelted by Flame or by Laser, *Wear*, 2007, **262**(3–4), p 301–307.
19. D. Kong and B. Zhao, Effects of Loads on Friction–Wear Properties of HVOF Sprayed NiCrBSi Alloy Coatings by Laser Remelting, *J. Alloys Compd.*, 2017, **705**, p 700–707.
20. L.-Y. Chen, T. Xu, S. Lu, Z.-X. Wang, S. Chen, and L.-C. Zhang, Improved Hardness and Wear Resistance of Plasma Sprayed Nanostructured NiCrBSi Coating Via Short-Time Heat Treatment, *J Surf. Coat. Technol.*, 2018, **350**, p 436–444.
21. T. Ungár, Microstructural Parameters from X-Ray Diffraction Peak Broadening, *Scripta Mater.*, 2004, **51**(8), p 777–781.
22. S. Liu, X. Zheng, and G. Geng, Dry Sliding Wear Behavior and Corrosion Resistance of NiCrBSi coating Deposited by Activated Combustion-High Velocity Air Fuel Spray Process, *Mater. Des.*, 2010, **31**(2), p 913–917.
23. L. Liu, H. Xu, J. Xiao, X. Wei, G. Zhang, and C. Zhang, Effect of Heat Treatment on Structure and Property Evolutions of Atmospheric Plasma Sprayed NiCrBSi Coatings, *J. Surf. Coat. Technol.*, 2017, **325**, p 548–554.
24. Š Houdková, E. Smazalová, M. Vostřák, and J. Schubert, Properties of NiCrBSi Coating, as Sprayed and Remelted by Different Technologies, *Surf. Coat. Technol.*, 2014, **253**, p 14–26.
25. J. Miguel, J. Guilemany, and S. Vizcaino, Tribological Study of NiCrBSi Coating Obtained by Different Processes, *Tribol. Int.*, 2003, **36**(3), p 181–187.
26. C. Navas, R. Colaco, J. De Damborenea, and R. Vilar, Abrasive Wear Behaviour of Laser Clad and Flame Sprayed-Melted NiCrBSi Coatings, *Surf. Coat. Technol.*, 2006, **200**(24), p 6854–6862.
27. N. Serres, F. Hlawka, S. Costil, C. Langlade, and F. Machi, An Investigation of the Mechanical Properties and Wear Resistance of NiCrBSi Coatings Carried Out by in Situ Laser Remelting, *Wear*, 2011, **270**(9–10), p 640–649.
28. A. Leyland and A. Matthews, On the Significance of the H/E Ratio in Wear Control: A Nanocomposite Coating Approach to Optimised Tribological Behaviour, *Wear*, 2000, **246**(1), p 1–11.
29. G. Bolelli and L. Lusvarghi, Heat Treatment Effects on the Tribological Performance of HVOF Sprayed Co-Mo-Cr-Si Coatings, *J. Thermal Spray Technol.*, 2006, **15**(4), p 802–810.
30. I. Hutchings, Tribology: friction and wear of engineering materials. 1992, Arnold, London, (1992)
31. A.D. Sarkar, *Wear of Metals: International Series in Materials Science and Technology*, Elsevier, 2013
32. G. Bolelli, Replacement of Hard Chromium Plating by Thermal Spraying–Problems, Solutions and Possible Future Approaches, *Surf. Eng.*, 2009, **25**(4), p 263–269.
33. A. Ibrahim and C. Berndt, Fatigue and Deformation of HVOF Sprayed WC–Co Coatings and Hard Chrome Plating, *Mater. Sci. Eng., A*, 2007, **456**(1–2), p 114–119.
34. A.C. Fischer-Cripps, *Introduction to Contact Mechanics*, Springer, 2000
35. M. Cadenas, R. Vijande, H. Montes, and J. Sierra, Wear Behaviour of Laser Cladded and Plasma Sprayed WC Co Coatings, *Wear*, 1997, **212**(2), p 244–253.

36. A. Conde and F. Zubiri, Cladding of Ni–Cr–B–Si Coatings with a High Power Diode Laser, *Mater. Sci. Eng., A*, 2002, **334**(1–2), p 233–238.
37. I. Garbar, Gradation of Oxidational Wear of Metals, *Tribol. Int.*, 2002, **35**(11), p 749–755.

Publisher's Note Springer Nature remains neutral with regard to jurisdictional claims in published maps and institutional affiliations.

Springer Nature or its licensor holds exclusive rights to this article under a publishing agreement with the author(s) or other rightsholder(s); author self-archiving of the accepted manuscript version of this article is solely governed by the terms of such publishing agreement and applicable law.